Polymer Chemistry

Accepted Manuscript

This is an *Accepted Manuscript*, which has been through the Royal Society of Chemistry peer review process and has been accepted for publication.

Accepted Manuscripts are published online shortly after acceptance, before technical editing, formatting and proof reading. Using this free service, authors can make their results available to the community, in citable form, before we publish the edited article. We will replace this *Accepted Manuscript* with the edited and formatted *Advance Article* as soon as it is available.

You can find more information about *Accepted Manuscripts* in the Information for Authors.

Please note that technical editing may introduce minor changes to the text and/or graphics, which may alter content. The journal's standard Terms & Conditions and the Ethical guidelines still apply. In no event shall the Royal Society of Chemistry be held responsible for any errors or omissions in this *Accepted Manuscript* or any consequences arising from the use of any information it contains.

ROYAL SOCIETY OF CHEMISTRY

www.rsc.org/polymers

Journal Name

ARTICLE

Multifunctional Hyperbranched Polymers for CT/^{19}F MRI Bimodal Molecular Imaging

Received 00th January 20xx,
Accepted 00th January 20xx

DOI: 10.1039/x0xx00000x

www.rsc.org/

Kewei Wang, Hui Peng, Kristofer J. Thurecht, Simon Puttick and Andrew K. Whittaker*

To develop novel contrast agents for bimodal molecular imaging, we report here the design and synthesis of multifunctional hyperbranched polymers containing iodine and fluorine and their application as CT/^{19}F MRI bimodal imaging contrast agents. A hyperbranched iodopolymer (HBIP), which was composed of 2-(2',3',5'-triiodobenzoyl)ethyl methacrylate (TIBMA), poly(ethylene glycol) methyl ether methacrylate (PEGMA) and a degradable crosslinker, was first synthesised by reversible addition-fragmentation chain transfer (RAFT) polymerization. Then the HBIP was chain extended with PEGMA and 2,2,2-trifluoroethyl acrylate (TFEA) to form hyperbranched iodopolymers containing ^{19}F (HBIPFs). A series of HBIPFs with different contents of iodine and fluorine were prepared. Nanoparticles with diameter of 10~15 nm were formed by direct dissolution of HBIPFs in water, and the biodegradability was revealed by the treatment of reducing agents. The radio-opacity of these nanoparticles in aqueous solution was confirmed by in vitro CT experiments, and solutions of the nanoparticles were visualised by ^{19}F MRI. These results suggest that the HBIPFs are attractive candidates for CT/^{19}F MRI bimodal imaging.

Introduction

In recent decades clinical diagnosis has advanced rapidly owing to the emergence of modern imaging techniques, such as magnetic resonance imaging (MRI), computed tomography (CT), positron emission tomography (PET), single photon emission computed tomography (SPECT), optical imaging, ultrasonography, etc. Although these techniques are frequently employed in the clinic and in research, each modality has its own advantages and limitations. For instance, optical imaging has high sensitivity but poor tissue penetration, while MRI provides high spatial resolution and no tissue penetration limitations but suffers from low sensitivity and relatively long imaging time.[1] Therefore, in some cases a single modality cannot offer sufficiently comprehensive data required for accurate diagnosis. In recognition of this the combination of two or more modalities has been a trend in both research and clinic applications in recent years.[2-5] Compared to single modality imaging, complementary information can be obtained through multimodal imaging, such as PET/CT, PET/MRI and optical/MRI, facilitating accurate diagnosis as well as assisting treatment.

The development of nanotechnology has brought enormous possibilities for the design of nanoparticle (NP)-based molecular imaging agents. Owing to the unique physicochemical properties of NPs, NP-based agents have a number of advantages compared with their small molecule counterparts, e.g. longer circulation time, integration of different functionalities, controllable size and surface properties, etc.[2, 6-8] In the past decade a significant range of NP-based multimodal imaging agents have been developed, and this has greatly bolstered the prospects of multimodal imaging techniques.[2, 9-11]

Magnetic resonance imaging (MRI) is a non-invasive and non-destructive imaging modality that can generate 3D anatomic images of patients with high resolution in particular for soft tissue. In contrast, X-ray CT can produce images with high spatial resolution for hard tissue but it has poor contrast for soft tissue. Therefore the synergetic application of MRI and CT is attractive as this can enhance the imaging capability. In recent years, considerable attention has been paid to the design of CT/MRI contrast agents.[12-21] Most proposed agents have been based on liposomes, inorganic NPs or polymer-containing hybrid NPs. Surprisingly, CT/MRI agents based on dendritic polymers including hyperbranched polymers (HBPs) and dendrimers have not been reported to this date, regardless of their advantages for nanomedicine such as long blood retention time, 3D globular structure, multifunctional sites for functionalisation, intramolecular cavity for drug loading, biocompatibility, biodegradability, etc.[22-26]

Since the first study in 1977,[27] ^{19}F MRI has been recognised as a promising complementary modality to ^{1}H MRI, which is currently the dominant MRI in routine clinic scans. ^{19}F MRI has a number of advantages, the most remarkable being the physiological rarity of ^{19}F in the human body which can

Australian Institute for Bioengineering and Nanotechnology; Centre for Advanced Imaging; ARC Centre of Excellence in Convergent Bio-Nano Science and Technology, The University of Queensland, St. Lucia, Queensland 4072, Australia
E-mail: a.whittaker@uq.edu.au; Fax: +61-7-33463973; Tel: +61-7-33463885
† Electronic Supplementary Information (ESI) available: ^{1}H and ^{13}C NMR spectra of the iodo-monomer and RAFT agent. See DOI: 10.1039/x0xx00000x

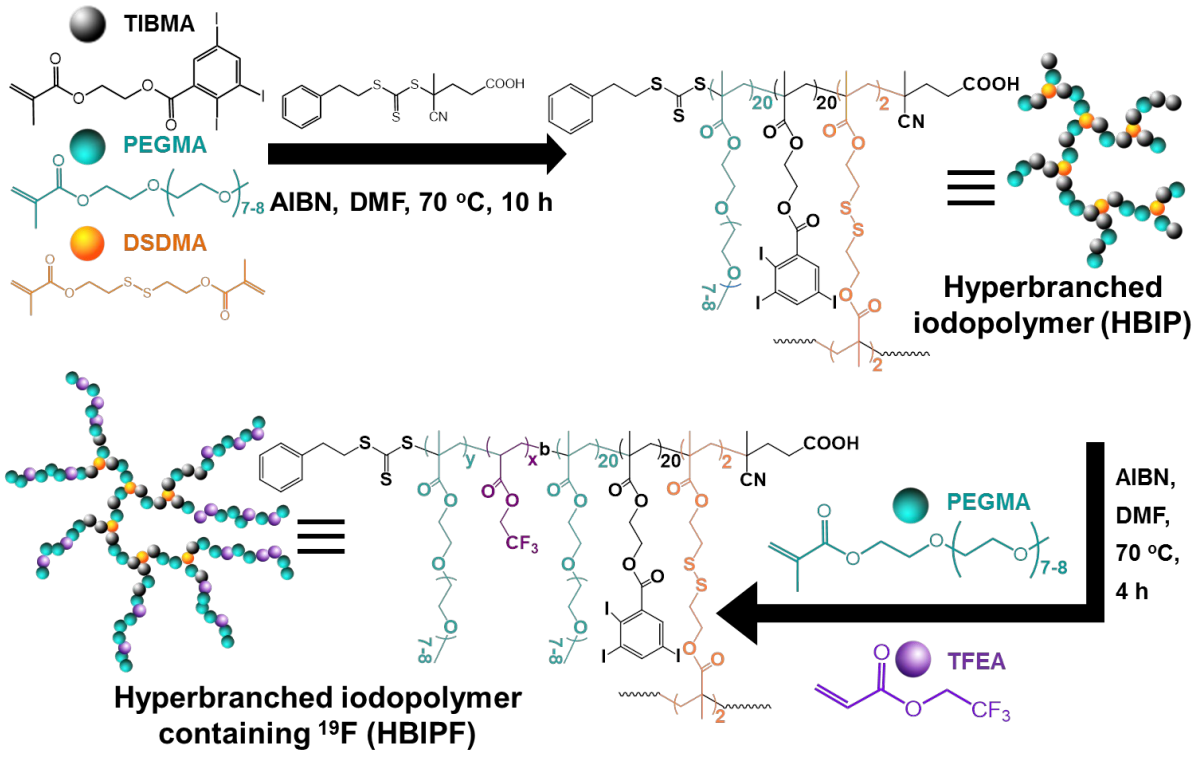

Scheme 1 Schematic illustration of the synthesis of hyperbranched polymers containing iodine and fluorine.

eliminate confounding background signals and thus generate selective ^{19}F MRI images.[28] In the past few years, polymeric ^{19}F MRI agents have attracted increasing attention. A wide range of ^{19}F-containing polymers have been synthesised and evaluated as ^{19}F MRI contrast agents, including linear polymers,[29-32] star polymers,[33, 34] hyperbranched and dendritic polymers,[35-41] nanogels,[42, 43] etc.

The combination of CT and ^{19}F MRI can allow for the imaging for hard tissue as well as the visualising of imaging probes. To the best of our knowledge, there is no literature reporting the design of CT/^{19}F MRI molecular imaging agents. Herein we report the design of multifunctional hyperbranched polymers containing iodine and fluorine and their application as CT/^{19}F MRI bimodal imaging contrast agents. The synthetic route is described in Scheme 1. In the first step, a hyperbranched iodopolymer (HBIP) was synthesised via reversible addition-fragmentation chain transfer (RAFT) polymerisation based on a previously reported procedure.[44] Specifically, the iodine-containing monomer, 2-(2',3',5'-triiodobenzoyl)ethyl methacrylate (TIBMA), was incorporated to introduce iodine atoms to provide X-ray opacity. The macromonomer, poly(ethylene glycol) methyl ether methacrylate (PEGMA, MW = 475 g mol^{-1}), was copolymerised to provide hydrophilicity. The disulfide-containing bifunctional monomer, bis2-(methacryloyl)oxyethyl disulfide (DSDMA), was chosen as a crosslinker to form branching structures and to achieve biodegradability. In the second step, the as-synthesised HBIP was used as a macro chain transfer agent (macro-CTA) and was chain extended with 2,2,2-trifluoroethyl acrylate (TFEA) and PEGMA. Finally hyperbranched iodopolymers containing ^{19}F (HBIPF) were obtained. According to the chemical structure, the iodine atoms were positioned within the branched inner part while the ^{19}F nuclei were dispersed in the outer copolymer chains. Since the polymers contained both iodine and fluorine, it was thus expect that they could be utilised as molecular imaging agents for CT/^{19}F MRI bimodal imaging.

The novelty of this work lies in the design of the first example of CT/^{19}F MRI bimodal molecular imaging agents as well as the development of multifunctional hyperbranched polymers as a promising platform for ^{19}F MRI-incorporated multimodal imaging.

Experimental Section

Materials

All chemicals were purchased from Sigma-Aldrich unless otherwise stated. Poly(ethylene) glycol methyl ether methacrylate (PEGMA, MW = 475 g mol^{-1}) and 2,2,2-trifluoroethyl acrylate (TFEA) were passed through basic alumina columns to remove inhibitors before use. 2,2'-Azobis(2-methylpropionitrile) (AIBN) was recrystallised twice from methanol prior to use. Bis(2-methacryloyl)oxyethyl disulfide (DSDMA) was synthesised following procedures published previously.[34, 45] The chain transfer agent (CTA), 4-cyano-4-(2-phenylethane sulfanylthiocarbonyl) sulfanylpentanoic acid (PETTC), was synthesised according to a previously reported method.[46] 4-(Dimethylamino)pyridine (DMAP), tris(2-carboxyethyl)phosphine hydrochloride (TCEP) and reduced L-glutathione (GSH) were used as received. N,N'-dicyclohexylcarbodiimide (DCC) were ordered from Alfa Aesar. Milli-Q water with a resistivity of 18.4 MΩ cm^{-1} was used for all the experiments that require water. Tetrahydrofuran (THF), dichloromethane (DCM) and N,N-dimethylformamide (DMF) were obtained from a solvent purification system (MB-SPS-800-Auto, Mbraun) and used directly. All other organic solvents were of analytical grade. Amicon ultra-15 centrifugal filter units (100k) were purchased from Merck Millipore.

Characterisation

Gel permeation chromatography (GPC). Molecular weights and molecular weight distributions were determined by GPC using a Waters Alliance 2690 Separations Module equipped with Waters 2414 Refractive Index (RI) Detector, Waters 2489 UV/Visible Detector, Waters 717 Plus Autosampler and Waters 1515 Isocratic HPLC Pump. Samples were dissolved in THF and passed through 0.45 μm filters before each measurement. THF was used as the mobile phase at a flow rate of 1 mL min^{-1}. The system was calibrated using polystyrene (PS) standards, to which the number average molecular weight (Mn) and weight average molecular weight (Mw) were referenced. For measuring absolute molecular weights, a multi angle laser light scattering (MALLS) detector (DAWN 8+, Wyatt) was attached to the GPC, and the polymer solutions were eluted at a flow rate of 1 mg mL^{-1} in THF. The refractive index increment (*dn*/*dc*) was determined by using ATAGO Pocket Refractometer at room temperature. Briefly, polymers were dissolved in THF at a range of concentrations from 10 to 300 mg mL^{-1}, and the refractive index of each solution was measured 5 times to get the average value. The *dn*/*dc* for each sample was calculated based on those values. The *dn*/*dc* values for HBIP and HBIPFs were 0.085 and 0.070, respectively.

Nuclear Magnetic Resonance (NMR). ^{1}H NMR and ^{13}C NMR were performed on a Bruker Avance 500 MHz spectrometer equipped with a BBO5 probe at 25 ^{o}C using an internal lock ($CDCl_3$) and referenced to the residual non-deuterated solvent ($CHCl_3$).

Dynamic Light Scattering (DLS). DLS measurements were carried out on a Nanoseries Zetasizer (Malvern, UK) at 25 ^{o}C. Sample solutions were prepared in PBS (1 mg mL^{-1}) at different pH values and passed through 0.45 μm filters prior to each measurement. Each hydrodynamic diameter was the average value of 5 measurements. To minimise the influence of large aggregates, number averaged diameters are reported.

Transmission Electron Microscopy (TEM). TEM experiments were conducted on a JOEL JEM-1010 transmission electron microscope at 80 kV. Samples were prepared by dropping polymer solutions (5 mg mL^{-1} in water) onto copper grids coated with glow discharged carbon, which were then left at room temperature overnight until dry. For each sample, a number of areas on the grid were examined and different magnifications were applied. Representative images are provided in this paper.

^{19}F Nuclear Magnetic Resonance (^{19}F NMR). All ^{19}F NMR spectra were acquired at 470.55 MHz without ^{1}H decoupling on a Bruker Avance 500 spectrometer using a 5 mm broadband inverse probe (BBO5) for which the inner coil was double-tuned for ^{19}F and ^{1}H. The samples were prepared by dissolving the star polymers in PBS/D_2O (90/10, v/v) at a concentration of 100 mg mL^{-1}. All measurements were performed at 25 ^{o}C. A 90o pulse of 15.1 μs was used in all measurements, the relaxation delay was 2 s and the acquisition time was 0.7 s. Data were collected using a spectrum width of 23 kHz, 32k data points and 128 scans.

^{19}F spin-spin relaxation times (T_2) were measured using the Carr-Purcell-Meiboom-Gill (CPMG) pulse sequence at 25 ^{o}C. The samples were dissolved in PBS/D_2O (90/10, v/v) at a concentration of 100 mg mL^{-1}. The relaxation delay was 3 s and the acquisition time was 0.7 s. For each measurement, the echo times were from 2 to 770 ms and 15 points were collected, which could be described by exponential functions for the calculation of T_2. Only values for the major peaks are reported.

^{19}F spin-lattice (T_1) relaxation times were measured using the standard inversion-recovery pulse sequence. For each measurement, the recovery times were from 2 ms to 3 s and 15 points were acquired. Only values for the major peaks are reported.

^{19}F Magnetic Resonance imaging (^{19}F MRI). Images of phantoms containing the solutions of the HBIPF nanoparticles were acquired on a Bruker BioSpec 94/30 USR 9.4 T small animal MRI scanner. HBIPFs were dissolved in PBS/D_2O (90/10,v/v) at different concentrations and were loaded in 30 × 8 mm clear vials， which were placed in a $^{1}H/^{19}F$ dual resonator 40 mm volume coil. ^{1}H images were acquired for localisation of the samples using a RARE sequence with an echo train length of 8 (TE = 28 ms, TR = 2 s, FOV = 40 × 40 × 1 mm, Matrix = 256 × 256 × 1). ^{19}F images were acquired in the same stereotactic space as the ^{1}H image using a RARE sequence with an echo train length of 8 (TE = 10 ms, effective TE = 40 ms, TR = 1 s, FOV = 40 × 40 × 10 mm, Matrix = 40 × 40 × 1, No. Averages = 256) and a total acquisition time of 21 minutes.

Computed Tomography (CT). Images of phantoms containing the solutions of the HBIPF nanoparticles were acquired on a Siemens Inveon Preclinical PET/CT scanner. HBPIFs were dissolved in PBS at different concentrations and

were loaded in 30 × 8 mm clear vials. Each sample was imaged individually to avoid the confounding of X-ray attenuation across the sample space. Each sample was placed in the centre of the X-ray field and images were acquired using an X-ray source with the voltage set to 80 kV and the current set to 500 µA. Scans were performed using 360° rotation with 180 rotation steps with low magnification and a binning factor of 4. Exposure time was 230 ms with an effective voxel size of 106 µm. CT images were reconstructed using the Cobra software package (Siemens) and normalised to a phantom containing pure water where Hounsfield units were set to 0 for pure water and -1000 for air.

Synthesis of 2-(2',3',5'-Triiodobenzoyl)ethyl Methacrylate (TIBMA)

TIBMA was prepared following an approach published elsewhere.[47, 48] Typically, 1,3,5-triiodobenzoic acid (10 g, 20 mmol), 2-hydroxyethyl methacrylate (5.2 g, 40 mmol) and DMAP (0.54 g, 4.4 mol) were mixed in 150 mL of DCM in a 500 mL flask. DCC (9.08 g, 44 mmol) in 50 mL of DCM was added dropwise to the above mixture over 10 min, and the solution was then stirred at room temperature for 24 h in the dark. After reaction, the mixture was filtered, and the filtrate was washed successively with HCl (2 M, 200 mL × 3) and saturated $NaHCO_3$ (200 mL × 3). Then the filtrate was dried over anhydrous $MgSO_4$, followed by filtration. The dark brown solution was collected and concentrated by rotary evaporation, then it was recrystallised from hexane/ethyl acetate (10/90, v/v) twice. Finally, the obtained pale soft powder was dried in vacuum at room temperature. Yield: 9.17 g, 75%. ^{1}H NMR (500 MHz, $CDCl_3$, ppm): 8.43 and 7.80 (2H, d, phenyl protons), 6.12 and 5.75 (2H, s, vinyl protons), 4.55 and 4.47 (4H, m, COOCH_2CH_2), 1.94 (3H, s, CH_3). ^{13}C NMR (125 MHz, $CDCl_3$, ppm): 166.80, 148.71, 142.47, 136.80, 127.25, 115.36, 108.16, 96.19, 64.81, 62.97, 18.91.

Synthesis of Hyperbranched Iodopolymer (HBIP)

The HBIP was synthesised by RAFT polymerisation. In a typical experiment, TIBMA (3.672 g, 6 mmol), PEGMA (2.85 g, 6 mmol), DSDMA (0.174 g, 0.6 mmol), PETTC (0.102 g, 0.3 mmol) and AIBN (4.92 mg, 0.03 mmol) were dissolved in 7.12 mL of DMF in a 50 mL flask. Next the flask was sealed with a rubber septum and purged with argon for 30 min in an ice bath. Then the flask was placed in a 70 °C oil bath and magnetically stirred for 10 h. After that the polymerisation was quenched by immersing the flask in ice bath and exposing it to air. The crude solution was precipitated into cold diethyl ether three times. Finally a brown viscous solid was obtained after drying in vacuum at room temperature. Yield: 6 g, 88%. GPC MALLS: M_n = 1.57 × 10^5 g mol^{-1}, molar mass dispersity ($Đ_M$, M_w/M_n) = 2.2.

Synthesis of Hyperbranched Iodopolymer Containing ^{19}F (HBIPF)

The HBIPF was prepared through chain extension of HBIPF with TFEA and PEGMA. By varying TFEA/PEGMA feed ratio, HBIPF-1, HBIPF-2 and HBIPF-3 with different compositions were synthesised. The synthesis of HBIPF-1 is described here as an example. HBIP (0.4 g, 2.55 ×10-3 mmol, equivalent to 0.018 mmol of CTA), TFEA (0.055 g, 0.36 mmol), PEGMA (0.684 g, 1.44 mmol) and AIBN (0.59 mg, 0.0036 mmol) were dissolved in 3.6 mL DMF in a 25 mL flask, which was then sealed with a rubber septum and purged with argon for 20 min in ice bath. After that the flask was placed in 70 °C oil bath and stirred for 4 h. Then the polymerisation was cooled down using an ice bath and exposed to air. The crude solution was precipitated into cold diethyl ether three times, and the collected polymer was further purified by centrifugal filtration (Amicon Ultra-15, 100k). After lyophilisation, a yellowish viscous solid was obtained. According to ^{1}H NMR, the monomer conversions of TFEA and PEGMA were 30% and 52%, respectively. GPC MALLS: M_n = 2.27 × 10^5 g mol^{-1}, molar mass dispersity ($Đ_M$, M_w/M_n) = 2.0. Yield: 0.65 g, 84%.

Degradation of HBIP Using Reducing Agents

In order to study the degradation using TCEP, HBIP (20 mg, 8.81 × 10^{-4} mmol) and TCEP (10.1 mg, 0.035 mmol) were dissolved in 1 mL methanol. The solution was purged with argon for 20 min and then stirred at room temperature for 24 h. An aliquot was sampled for GPC analysis.

For the treatment by GSH, HBIP (20 mg, 8.81 × 10^{-4} mmol) and GSH (21.6 mg, 0.07 mmol) were dissolved in 7 mL of PBS. The concentration of GSH was 10 mM. The solution was purged with argon for 20 min and then stirred at room temperature for 24 h. An aliquot was withdrawn and lyophilised for GPC analysis.

Results and Discussion

Synthesis of Partly-fluorinated Hyperbranched Iodopolymers

Since the pioneer work reported by Davy and co-workers,[47, 49] 2-(2',3',5'-triiodobenzoyl)ethyl methacrylate (TIBMA) has drawn much attention as a typical iodo-monomer for the synthesis of X-ray-opaque polymeric materials.[16, 48, 50-56] To date, most of the TIBMA-based polymeric agents have been microparticles prepared by conventional free radical polymerisation, whereas there are very few reports of TIBMA-based polymeric agents with hyperbranched or dendritic structures synthesised by controlled radical polymerisation.[57, 58] As introduced above, hyperbranched polymers possess a number of unique advantages, thus it is desirable to explore the synthesis of TIBMA-based hyperbranched polymers. These can be prepared via controlled polymerisation methods such as RAFT polymerisation,[59] which can be utilised for the synthesis of well-defined and complex architectures.[60, 61] As the TIBMA homopolymer is hydrophobic, it is important to increase the hydrophilicity by copolymerisation with PEGMA. This approach introduces polyethylene glycol side chains and has been widely used for preparing hydrophilic and biocompatible materials.[62] Furthermore, the crosslinker DSDMA used here contains a disulfide bond that can be

Table 1 GPC and ^{1}H NMR data for the HBIP and HBIPFs.

Sample	TIBMA/PEGMA/DSDMA in first block[a]	TFEA/PEGMA in second block[a]	M_n (each chain, kDa)[b]	Absolute M_n (kDa)[c]	$Đ_M$[c]	N_{CTA}[d]
HBIP	20/20/2	–	22.7	157	2.2	7
HBIPF-1	20/20/2	10/45	45.6	227	2.0	5
HBIPF-2	20/20/2	10/34	40.4	238	2.0	6
HBIPF-3	20/20/2	37/52	53.0	207	2.0	4

[a] Degree of polymerisation (DP) was obtained from ^{1}H NMR results. [b] M_n for each chain was calculated based on ^{1}H NMR. [c] Absolute molecular weight was measured by GPC MALLS. [d] Number of CTA functionalities per each molecule was estimated through the equation (N_{CTA}) = M_n (GPC MALLS)/M_n (^{1}H NMR),[35, 63] presuming that the branched structure was formed by inter-chain reaction rather than intra-chain cyclisation.

cleaved in the presence of reducing agents,[64-66], facilitating the removal of the polymers from the body for in vivo applications.

The iodo-monomer TIBMA was synthesised by the esterification between 1,3,5-triiodobenzoic acid and 2-hydroxyethyl methacrylate, and was purified by recrystallisation (see Fig. S1 for ^{1}H and ^{13}C NMR spectra). The RAFT agents PETTC was chosen because of the well-resolved peaks of its two aromatic protons at 8.43 and 7.80 ppm, facilitating the determination of degree of polymerisation by ^{1}H NMR (see Fig. S2 for ^{1}H and ^{13}C NMR spectra). Hyperbranched iodopolymers (HBIPs) were synthesised from the monomers TIBMA, PEGMA and DSDMA via RAFT polymerisation. The feed ratio of TIBMA/PEGMA/DSDMA/PETTC/AIBN was set to be 20/20/2/1/0.1. During the polymerisation, the conversion of the three monomers was monitored by ^{1}H NMR, and reached above 97% within 10 hours, indicating a fast rate of polymerisation. As listed in Table 1, the as-synthesised HBIP had an absolute Mn of 157 kDa with a relatively low (for a hyperbranched structure) molar mass dispersity, $Đ_M$, of 2.2. For each HBIP molecule, the number of CTA functionalities (N_{CTA}) was calculated to be 7, confirming the highly branched structure of the HBIP.

The HBIP was then used as a macro-CTA and chain extended with TFEA and PEGMA for the synthesis of hyperbranched iodopolymers containing ^{19}F (HBIPF). To investigate the effect of fluorine content on the ^{19}F MRI performance, three feed ratios of TFEA/PEGMA/CTA were used, i.e. 20/80/1, 40/80/1 and 80/80/1. The polymerisations were allowed to proceed for 4 hours, and the conversions of TFEA and PEGMA were approximately 30% and 52%, respectively. The resultant HBIPF samples with different TFEA/PEGMA compositions were denoted as HBIPF-1, HBIPF-2 and HBIPF-3, respectively. As shown in Table 1, all the HBIPFs had larger M_n than the HBIP macro-CTA, meanwhile the $Đ_M$ still kept low at 2.0,

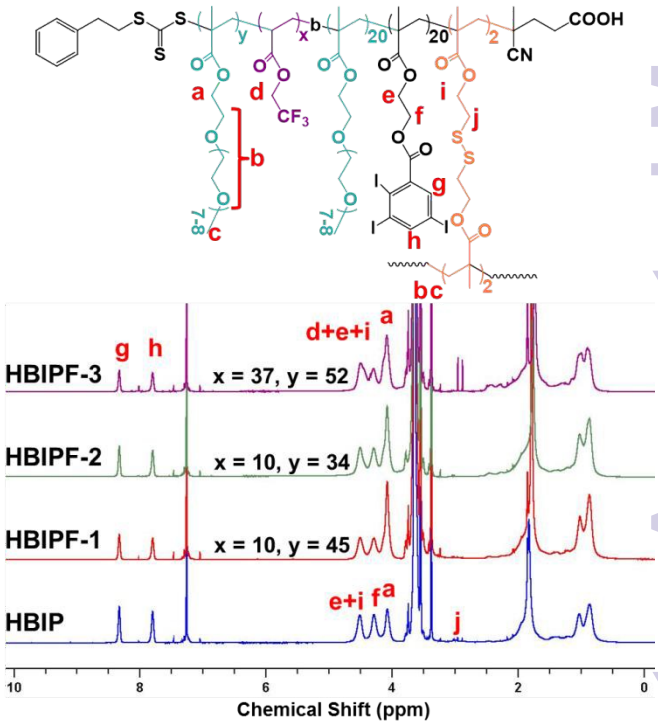

Fig. 1 ^{1}H NMR spectra of HBIP and HBIPFs in $CDCl_3$ at 25 ^oC.

demonstrating successful chain extension of HBIP via RAFT polymerisation.

As displayed in Fig. 1, the chemical structures of HBIP and HBIPFs were characterised by ^{1}H NMR. Specific peaks in the spectra were assigned to protons of TIBMA, PEGMA and DSDMA, as shown in the spectra. For all the samples, the protons of the aromatic ring were observed at 7.8 and 8.3 ppm, respectively. In addition, for the samples after chain extension, the peak of the two protons in the methylene group adjacent to -CF_3 was found to be overlapped with the peaks at 4.4~4.7 ppm, however the integral of this peak became larger with increasing TFEA/PEGMA feed ratio, suggesting an

Table 2 Properties of HBIP and HBIPFs.

Sample	I wt%[a] of each molecule	^{19}F wt%[a] of each molecule	^{19}F wt%[a] of the second block	T_1 (ms)[b]	T_2 (ms)[b]	D_h (nm)[c]
HBIP	33.6	0	-	-	-	12.24±2.31
HBIPF-1	17.0	1.3	2.5	405	61	13.49±1.05
HBIPF-2	19.0	1.4	3.2	374	38	13.09±1.28
HBIPF-3	14.4	4.0	6.9	102	11	12.45±1.03

[a] Iodine and fluorine weight percentages were calculated based on ^{1}H NMR results. [b] T_1 and T_2 of ^{19}F were determined by ^{19}F NMR.
[c] Hydrodynamic diameter (D_h) was measured by DLS in water at 25 °C.

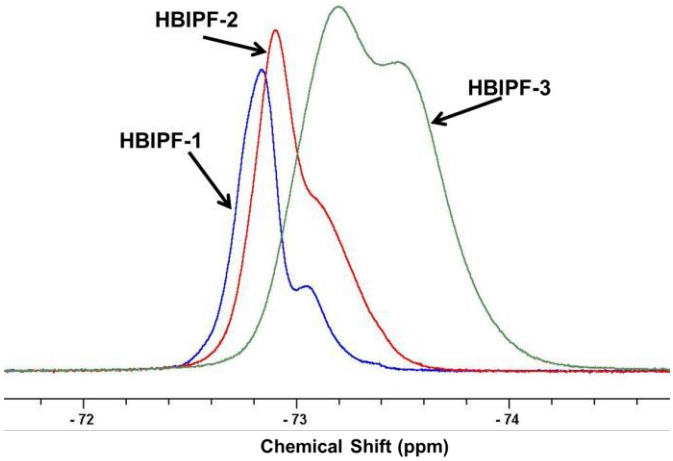

Fig. 2 ^{19}F NMR spectra of HBIPFs.

increasing amount of TFEA incorporated into the second block. Therefore, ^{1}H NMR results revealed the chemical structures of the samples and confirmed the successful chain extension of HBIP. Based on ^{1}H NMR results, the DP of each polymer chain was calculated and the content of iodine and fluorine was obtained. As listed in Table 2, the iodine content of HBIPFs was relatively constant at 17 ± 2.5 wt%. The weight percentages of ^{19}F of both the polymer and the second block were also provided in Table 2. The fluorine content of the polymer is required for the determination of ^{19}F concentration for ^{19}F MRI. However, the fluorine content of the second block is crucial for the study of ^{19}F NMR properties of the polymers because it can directly affect the mobility of ^{19}F nuclei in aqueous solution.

Examination of ^{19}F NMR Properties

The HBIPFs were also characterised by ^{19}F NMR. As shown in Fig. 2, the peaks at -72~-74.4 ppm confirmed the presence of ^{19}F in the HBIPFs. The bimodal nature of the peaks indicated that there are possibly two chemical environments for the ^{19}F nuclei. We propose that this is due to different sequence distributions caused by the largely different reactivity ratios of TFEA/PEGMA (0.22 and 2.46, respectively).[67] Hence, segments of PTFEA homopolymer and P(TFEA-co-PEGMA) statistical copolymer co-existed in the second block, resulting in two ^{19}F resonances.[68] Furthermore, the peak width also increased with ^{19}F content, indicating that the ^{19}F nuclei are experiencing stronger dipolar coupling at higher ^{19}F content. The spin-lattice relaxation time (T_1) and spin-spin relaxation time (T_2), which are two important parameters for ^{19}F MRI, were also determined by ^{19}F NMR. As displayed in Table 2, when the fluorine content was increased from 0.6 to 4.0 wt%, T_2 dropped from 61 to 11 ms. We previously reported that T_2 could be significantly affected by the ^{19}F content of similar polymers because of the hydrophobic nature of the fluorinated segments.[31, 33, 34] To be more specific, in aqueous solution, a high fluorine content can induce aggregation of these units, which reduces the mobility of the ^{19}F nuclei resulting in short T_2 values. In our previous work, it was observed that T_1 was not greatly affected by the change in polymer dimensions.[33, 34] However, in this work, the T_1 of HBIPF-3 was measured to be 102 ms, which is much shorter than those of HBIPF-1 and 2. This is not surprising because T_1 generally decreases with T_2 in a certain range of correlation time in a fixed magnetic field.[69] We thus assume that T_1 could be significantly related to the composition or tacticity of the copolymer chain. Since long T_2 and short T_1 relaxation times are preferred for spin-echo imaging,[30] it is essential to not only achieve high fluorine content but also prevent the fluorine nuclei from associating strongly.

Studies of Morphology

Owing to the incorporation of significant concentrations of hydrophilic PEGMA monomer units, the as synthesised HBIP and HBIPFs were water soluble. Nanoparticles could be formed by direct dissolution of the polymers in water (1 mg mL^{-1}), and the particle size was measured by dynamic light scattering (DLS) at 25 °C. As shown in Table 2, the number-averaged diameter of all three HBIPFs was approximately 13 nm, which was slightly larger than that of the HBIP, indicating an increased size after chain extension. The size and morphology were also studied by transmission electron microscopy (TEM) (Fig. 3), and the majority of HBIPF-1 nanoparticles exhibited a size of ~6 nm, which was smaller than the size provided by

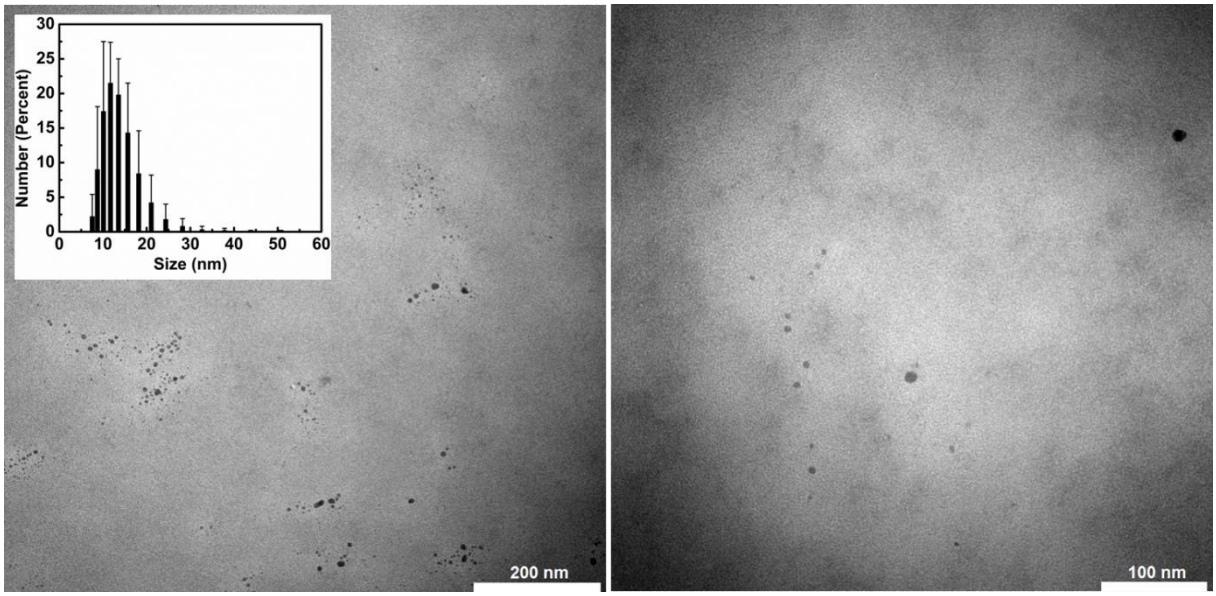

Fig. 3 Representative TEM images of HBIPF-1 nanoparticles in water. Inset is the number-averaged size statistics graph acquired by DLS.

DLS. This is because DLS determines the hydrodynamic diameter of the nanoparticles in aqueous solution, which is generally larger than the size of dehydrated samples observed by TEM experiments.[70] Moreover, a number of large particles (~12 nm) were also found in the TEM images. We propose that a small amount of aggregations were formed owing to the hydrophobic nature of fluorine and iodine units. Hence it could be concluded that the HBPIFs could form nanoparticles with size of ~13 nm in aqueous solution.

Degradation of HBIP in Reducing Environment

As mentioned above, the crosslinker DSDMA contains a disulfide bond that is cleavable in the presence of reducing agents. Therefore the HBIP and HBIPFs are expected to be biodegradable. Test of the degradability were carried out by using either TCEP or GSH as reducing agents, and the resultant polymers were characterised by GPC. As shown in Fig. 4, the original HBIP showed bimodal GPC peaks with retention times of 14.4 and 15.6 min, which is a typical characteristic of hyperbranched polymers synthesised by controlled radical polymerisation in the presence of crosslinkers.[44, 71, 72] After being treated with TCEP in methanol for 24 h, the peak at shorter retention time (14.4 min) almost disappeared, and only a single peak at longer retention time (15.6 min) was observed, demonstrating degradation of the hyperbranched structure via cleavage of disulfide bonds. Similarly, the HBIP was also treated with GSH at a physiological concentration (10 mM)[73] in PBS for 24 h, and the majority of the hyperbranched polymers were degraded. It should be noted that the small peak at 13.2 min arises from polymers formed by re-formation of inter-molecular disulphide bonds on the degraded fragments. We assume that the lower degradation efficiency of GSH was caused by the relatively low concentration of

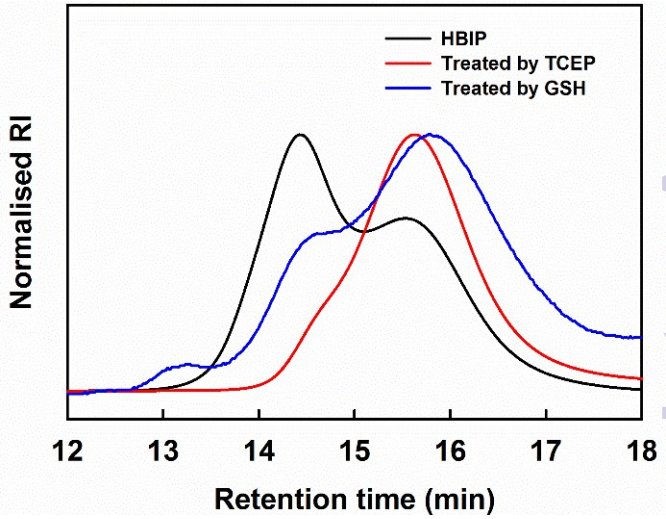

Fig. 4 GPC traces for HBIP before and after treatment by TCEP and GSH.

reducing agent. Overall, the GPC results confirmed that incorporation of the crosslinker DSDMA can impart biodegradability to the hyperbranched polymers.

Imaging performance: X-ray CT and ^{19}F MRI

The imaging performance of the HBIPFs was evaluated by in vitro X-ray CT and ^{19}F MRI experiments. Each sample was dissolved in PBS at four different concentrations and loaded in clear glass vials (8 × 30 mm, 0.75 mL) for imaging tests. The detailed concentrations and results are listed in Table 3.

Table 3 Sample concentrations, CT values and signal-to-noise ratio (SNR) of ^{19}F MRI.

Sample	[Polymer]	[I]		[^{19}F]		CT values	^{19}F MRI
	mg mL^{-1}	mg mL^{-1}	M	mg mL^{-1}	M	(HU)	SNR
HBIPF-1	11.2	1.9	0.015	0.07	0.004	18.8±32.3	1.96
	22.4	3.8	0.030	0.14	0.008	66.3±30.4	2.55
	56	9.5	0.075	0.36	0.019	278.3±30.3	7.77
	112	19	0.150	0.72	0.038	571.9±30.9	10.83
HBIPF-2	10	1.9	0.015	0.10	0.005	33.6±28.8	2.30
	20	3.8	0.030	0.20	0.010	90.6±28.5	23.23
	50	9.5	0.075	0.50	0.025	304±29.8	9.82
	100	19	0.150	1.00	0.050	591.6±30.4	15.29
HBIPF-3	13.2	1.9	0.015	0.53	0.028	2.6±30.4	2.67
	26.4	3.8	0.030	1.06	0.056	46.3±32.8	4.21
	52.8	7.6	0.060	2.11	0.111	167.1±31.3	9.07
	105.6	15.2	0.120	4.22	0.222	333.1±30.9	14.75

Owing to the high atomic number, and hence high x-ray cross-section of iodine, iodine-based materials have been extensively studied for CT molecular imaging.[74] In recent years, iodine-containing particles and polymers have drawn much attention, such as liposomes,[75, 76] emulsion particles,[77-79] block copolymer micelles,[58] coordination polymers,[80] etc. However, data on dendritic polymer-based agents is scarce. In this work, the radio-opacity of the HBIPFs was evaluated by in vitro CT experiments using an Inveon PET/CT scanner (Siemens). As shown in Fig. 5 (A), all the sample solutions exhibited X-ray opacity, which increased with the polymer concentration. In addition, the CT attenuation (in Hounsfield units) of the region of interest (ROI) showed a linear relationship with iodine concentration (Fig. 5 (B)).

In a previous report, iodinated polymeric nanoparticles (58 wt% Iodine) were prepared using the same iodine-containing monomer by emulsion polymerisation.[54] The radio-opacification was measured to be 362±1 HU for the nanoparticle dispersion at 16 mg mL^{-1} in water (equals to 9.28 mg mL^{-1} iodine). In another paper, an emulsion based on iodinated oils was fabricated and stabilised by block copolymers.[79] These nanoparticles were utilised for in vivo CT and tested using mouse models. The CT values for blood, spleen and liver were measured after injection. It was observed that the CT value was proportional to the iodine concentration in the organs, which was calculated from the change in the CT values. For example, the CT values for iodine concentrations of 10 and 20 mg ml^{-1} were 310±20 and ~620±40 HU, respectively. In our work, the CT values for the sample with 9.5 mg mL^{-1} iodine were 278.3±30.3 HU and 304±29.8 HU for HBIPF-1 and HBIPF-2, respectively, while the CT values for the sample with 19 mg mL^{-1} iodine were measured to be 571.9±30.9 HU and 591.6±30.4 HU for HBIPF-1 and HBIPF-2, respectively. Because the CT values for specific iodine concentrations were close to those reported in the literatures, we suggest that the radio-opacity of the iodinated

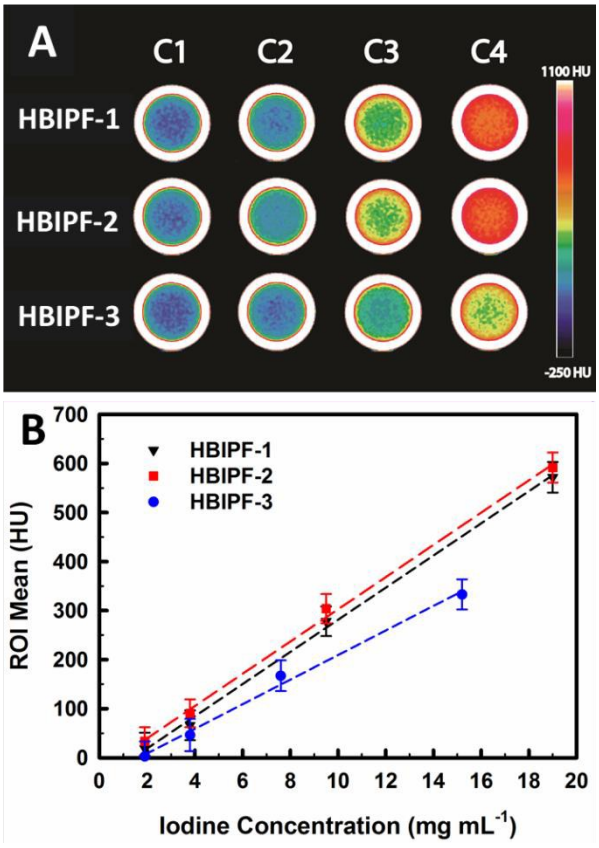

Fig. 5 (A) In vitro CT phantom images of HBIPFs aqueous solutions with different iodine concentrations. For HBIPF-1 and HBIPF-2, C1 = 0.015 M, C2 = 0.030 M, C3 = 0.075 M, C4 = 0.150 M. For HBIPF-3, C1 = 0.015 M, C2 = 0.030 M, C3 = 0.060 M, C4 = 0.120 M. (B) The corresponding CT values of ROI as a function of iodine concentration.

polymers was only related to the iodine concentration, and was not significantly affected by the architecture, morphology or composition of the polymeric materials. Notably, the CT values of in vitro and in vivo studies were relatively close, similarly suggesting that the radio-opacity was not affected by the physiological environment. Therefore these results confirm that the HBIPFs have the potential for application as in vivo CT agents.

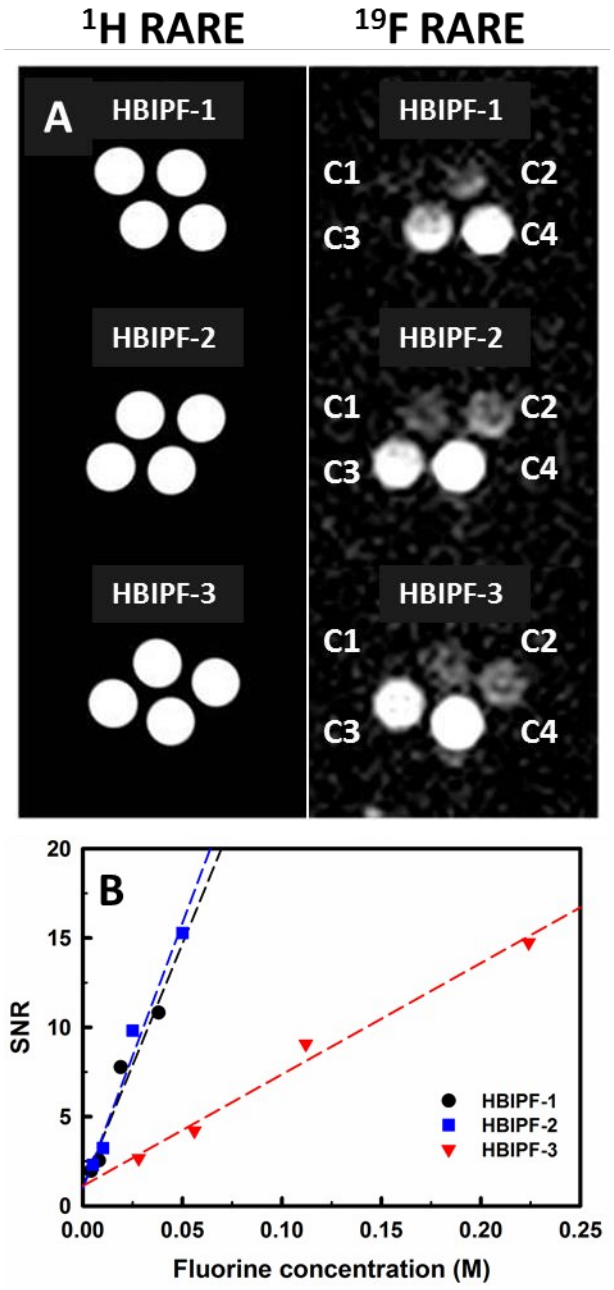

Fig. 6 (A) In vitro ^{19}F MRI phantom images of aqueous solutions of HBIPFs at different fluorine concentrations. The concentrations are the same as those in Fig. 5. Note: ^{1}H RARE images were used for the localisation of the field of view. (B) Signal-to-noise ratio (SNR) in ^{19}F MRI as a function of fluorine concentration.

The NMR detectable ^{19}F nuclei were confirmed by ^{19}F NMR, indicating that the HBIPFs developed here could have potential as contrast agents for ^{19}F MRI. The same solutions of HBIPFs examined by x-ray CT were assessed by ^{19}F MRI. As depicted in Fig. 6 (A), the HBIPF nanoparticles provided positive signals at all concentrations. When the fluorine concentration was relatively high (C3 and C4 for all the samples), the nanoparticles could be particularly well imaged. From Fig. 6 (B), one can see that the signal-to-noise ratio (SNR) was directly proportional to fluorine content. Moreover, the SNR for HBIPF-2 was slightly higher than that of HBIPF-1 because of the increase in fluorine content from 0.64% to 1%. However, the SNR for HBIPF-3 was significantly lower than for the other samples. This can be explained by the considerably increased fluorine content (4%) causing aggregation of fluorine nuclei in water and thus resulting in greatly shortened T_2 relaxation times, as was revealed by ^{19}F NMR.

As studied before, the T_2 relaxation time was shortened with the increase of ^{19}F content of the polymers due to the increased association of ^{19}F segments in aqueous solution.[33, 34] For example, at pH 4~7.4, the T_2s of the sample CCS-2 (3.9 wt% of ^{19}F) were nearly half of those of the sample CCS-1 (2.3 wt% of ^{19}F), indicating the dramatically increased aggregation of ^{19}F units at higher ^{19}F content. Consequently, the ^{19}F MRI SNR of CCS-2 was significantly lower than that of CCS-1.[34] In this work, similar results were obtained. The observation of lowest SNR of HBIPF-3 is in accord with previous findings, supporting that long T_2s (mobile ^{19}F nuclei) are preferred for spin-echo imaging. However, the SNR of HBIPF-2 (1 wt% of ^{19}F, T_2 = 38 ms) was slightly higher than that of HBIPF-1 (0.6 wt% of ^{19}F, T_2 = 61 ms), confirming that ^{19}F concentration was also another crucial factor for ^{19}F MRI. Therefore both high ^{19}F content and long T_2 are prerequisite for the design of ^{19}F MRI CAs with high efficiency.

Conclusions

In conclusion, multifunctional hyperbranched polymers containing iodine and fluorine were synthesised via RAFT polymerisation. The content of iodine and fluorine could be tuned by varying the monomer feed ratio for the chain extension reaction. The HBIPFs could be degraded by treatment of reducing agents such as GSH and TCEP, and thus the polymer would be likely excreted in vivo. By direct dissolution of the HBIPFs in water, nanoparticles were formed with diameters between 10~15 nm. In aqueous solution, the radio-opacity of these nanoparticles was confirmed by in vitro CT experiments. In addition, solutions of the nanoparticles could be visualised by ^{19}F MRI. These results suggest that the HBIPFs are promising molecular imaging agents for CT/^{19}F MRI bimodal imaging.

Acknowledgements

The authors would like to acknowledge the Australian Research Council (CE140100036, DP0987407, DP110104299, LE0775684, LE0668517, and LE0882357) for funding of this research. The Australian National Fabrication Facility, Queensland Node is also acknowledged for access to some items of equipment. H.P. thanks the University of Queensland for her UQ Postdoctoral Research Fellowship for Women.

Notes and references

1. J. K. Willmann, N. van Bruggen, L. M. Dinkelborg and S. S. Gambhir, *Nat Rev Drug Discov*, 2008, **7**, 591-607.
2. D. E. Lee, H. Koo, I. C. Sun, J. H. Ryu, K. Kim and I. C. Kwon, *Chem Soc Rev*, 2012, **41**, 2656-2672.
3. L. E. Jennings and N. J. Long, *Chem Commun*, 2009, DOI: Doi 10.1039/B821903f, 3511-3524.
4. S. R. Cherry, *Annu Rev Biomed Eng*, 2006, **8**, 35-62.
5. A. Y. Louie, *Chem Rev*, 2010, **110**, 3146-3195.
6. X. Hu, G. Liu, Y. Li, X. Wang and S. Liu, *Journal of the American Chemical Society*, 2014, **137**, 362-368.
7. G. Liu, G. Zhang, J. Hu, X. Wang, M. Zhu and S. Liu, *Journal of the American Chemical Society*, 2015, **137**, 11645-11655.
8. X. Li, Y. Qian, T. Liu, X. Hu, G. Zhang, Y. You and S. Liu, *Biomaterials*, 2011, **32**, 6595-6605.
9. G. Bao, S. Mitragotri and S. Tong, *Annual Review of Biomedical Engineering, Vol 15*, 2013, **15**, 253-282.
10. P. A. Jarzyna, A. Gianella, T. Skajaa, G. Knudsen, L. H. Deddens, D. P. Cormode, Z. A. Fayad and W. J. M. Mulder, *Wires Nanomed Nanobi*, 2010, **2**, 138-150.
11. J. Cheon and J. H. Lee, *Accounts Chem Res*, 2008, **41**, 1630-1640.
12. M. Lijowski, S. Caruthers, G. Hu, H. Y. Zhang, M. J. Scott, T. Williams, T. Erpelding, A. H. Schmieder, G. Kiefer, G. Gulyas, P. S. Athey, P. J. Gaffney, S. A. Wickline and G. M. Lanza, *Invest Radiol*, 2009, **44**, 15-22.
13. J. Z. Zheng, J. B. Liu, M. Dunne, D. A. Jaffray and C. Allen, *Pharm Res-Dordr*, 2007, **24**, 1193-1201.
14. D. Kim, M. K. Yu, T. S. Lee, J. J. Park, Y. Y. Jeong and S. Jon, *Nanotechnology*, 2011, **22**.
15. S. W. Chou, Y. H. Shau, P. C. Wu, Y. S. Yang, D. B. Shieh and C. C. Chen, *J Am Chem Soc*, 2010, **132**, 13270-13278.
16. A. Hagit, B. Soenke, B. Johannes and M. Shlomo, *Biomacromolecules*, 2010, **11**, 1600-1607.
17. L. J. Wang, H. Y. Xing, S. J. Zhang, Q. G. Ren, L. M. Pan, K. Zhang, W. B. Bu, X. P. Zheng, L. P. Zhou, W. J. Peng, Y. Q. Hua and J. L. Shi, *Biomaterials*, 2013, **34**, 3390-3401.
18. M. Beija, Y. Li, H. T. Duong, S. Laurent, L. Vander Elst, R. N. Muller, A. B. Lowe, T. P. Davis and C. Boyer, *J Mater Chem*, 2012, **22**, 21382-21386.
19. S. Narayanan, B. N. Sathy, U. Mony, M. Koyakutty, S. V. Nair and D. Menon, *Acs Appl Mater Inter*, 2012, **4**, 251-260.
20. C. Alric, J. Taleb, G. Le Duc, C. Mandon, C. Billotey, A. Le Meur-Herland, T. Brochard, F. Vocanson, M. Janier, P. Perriat, S. Roux and O. Tillement, *J Am Chem Soc*, 2008, **130**, 5908-5915.
21. D. P. Cormode, T. Skajaa, M. M. van Schooneveld, R. Koole, P. Jarzyna, M. E. Lobatto, C. Calcagno, A. Barazza, R. E. Gordon, P. Zanzonico, E. A. Fisher, Z. A. Fayad and W. J. M. Mulder, *Nano Lett*, 2008, **8**, 3715-3723.
22. Y. F. Zhou, W. Huang, J. Y. Liu, X. Y. Zhu and D. Y. Yan, *Adv Mater*, 2010, **22**, 4567-4590.
23. H. B. Jin, W. Huang, X. Y. Zhu, Y. F. Zhou and D. Y. Yan, *Chem Soc Rev*, 2012, **41**, 5986-5997.
24. S. Sevenson and D. A. Tomalia, *Adv Drug Deliver Rev*, 2012, **64**, 102-115.
25. C. M. Paleos, D. Tsiourvas, Z. Sideratou and L. A. Tziveleka, *Expert Opin Drug Del*, 2010, **7**, 1387-1398.
26. C. M. Paleos, L. A. Tziveleka, Z. Sideratou and D. Tsiourvas, *Expert Opin Drug Del*, 2009, **6**, 27-38.
27. G. N. Holland, P. A. Bottomley and W. S. Hinshaw, *Journal of Magnetic Resonance*, 1977, **28**, 133-136.
28. J. Ruiz-Cabello, B. P. Barnett, P. A. Bottomley and J. W. Bulte, *NMR Biomed*, 2011, **24**, 114-129.
29. H. Peng, K. J. Thurecht, I. Blakey, E. Taran and A. K. Whittaker, *Macromolecules*, 2012, **45**, 8681-8690.
30. H. Peng, I. Blakey, B. Dargaville, F. Rasoul, S. Rose and A. K. Whittaker, *Biomacromolecules*, 2009, **10**, 374-381.
31. L. Nurmi, H. Peng, J. Seppala, D. M. Haddleton, I. Blakey and A. K. Whittaker, *Polymer Chemistry*, 2010, **1**, 1039-1047.
32. X. N. Huang, G. Huang, S. R. Zhang, K. Sagiyama, O. Togao, X. P. Ma, Y. G. Wang, Y. Li, T. C. Soesbe, B. D. Sumer, M. Takahashi, A. D. Sherry and J. M. Gao, *Angewandte Chemie-International Edition*, 2013, **52**, 8074-8078.
33. K. W. Wang, H. Peng, K. J. Thurecht, S. Puttick and A. K. Whittaker, *Polymer Chemistry*, 2013, **4**, 4480-4489.
34. K. Wang, H. Peng, K. J. Thurecht, S. Puttick and A. K. Whittaker, *Polymer Chemistry*, 2014, **5**, 1760.
35. K. J. Thurecht, I. Blakey, H. Peng, O. Squires, S. Hsu, C. Alexander and A. K. Whittaker, *J Am Chem Soc*, 2010, **132**, 5336-5337.
36. M. Ogawa, S. Nitahara, H. Aoki, S. Ito, M. Narazaki and T. Matsuda, *Macromol Chem Phys*, 2010, **211**, 1369-1376.
37. M. Ogawa, S. Nitahara, H. Aoki, S. Ito, M. Narazaki and T. Matsuda, *Macromolecular Chemistry and Physics*, 2010, **211**, 1602-1609.
38. W. J. Du, A. M. Nystrom, L. Zhang, K. T. Powell, Y. L. Li, C. Cheng, S. A. Wickline and K. L. Wooley, *Biomacromolecules*, 2008, **9**, 2826-2833.
39. W. J. Du, Z. Q. Xu, A. M. Nystrom, K. Zhang, J. R. Leonard and K. L. Wooley, *Bioconjugate Chemistry*, 2008, **19**, 2492-2498.
40. J. M. Criscione, B. L. Le, E. Stern, M. Brennan, C. Rahner, X. Papademetris and T. M. Fahmy, *Biomaterials*, 2009, **30**, 3946-3955.
41. C. Porsch, Y. N. Zhang, A. Ostlund, P. Damberg, C. Ducani, E. Malmstrom and A. M. Nystrom, *Particle & Particle Systems Characterization*, 2013, **30**, 381-390.
42. M. Oishi, S. Sumitani and Y. Nagasaki, *Bioconjugate Chemistry*, 2007, **18**, 1379-1382.
43. M. M. Bailey, C. M. Mahoney, K. E. Dempah, J. M. Davis, M. L. Becker, S. Khondee, E. J. Munson and C. Berkland, *Macromolecular Rapid Communications*, 2010, **31**, 87-92.
44. B. L. Liu, A. Kazlauciunas, J. T. Guthrie and S. Perrier, *Macromolecules*, 2005, **38**, 2131-2136.
45. Y. T. Li and S. P. Armes, *Macromolecules*, 2005, **38**, 8155-8162.

46. M. Semsarilar, V. Ladmiral, A. Blanazs and S. P. Armes, *Langmuir*, 2012, **28**, 914-922.
47. K. W. M. Davy, M. R. Anseau, M. Odlyha and G. M. Foster, *Polym Int*, 1997, **43**, 143-154.
48. A. Galperin and S. Margel, *J Polym Sci Pol Chem*, 2006, **44**, 3859-3868.
49. K. W. M. Davy, M. R. Anseau and C. Berry, *J Dent*, 1997, **25**, 499-505.
50. K. Saralidze, Y. B. J. Aldenhoff, M. L. W. Knetsch and L. H. Koole, *Biomacromolecules*, 2003, **4**, 793-798.
51. A. Artola, M. Gurruchaga, B. Vazquez, J. San Roman and I. Goni, *Biomaterials*, 2003, **24**, 4071-4080.
52. C. Zaharia, T. Zecheru, M. F. Moreau, F. Pascaretti-Grizon, G. Mabilleau, B. Marculescu, R. Filmon, C. Cincu, G. Staikos and D. Chappard, *Acta Biomater*, 2008, **4**, 1762-1769.
53. H. Aviv, S. Bartling, F. Kieslling and S. Margel, *Biomaterials*, 2009, **30**, 5610-5616.
54. A. Galperin, D. Margel, J. Baniel, G. Dank, H. Biton and S. Margel, *Biomaterials*, 2007, **28**, 4461-4468.
55. A. Galperin and S. Margel, *Biomacromolecules*, 2006, **7**, 2650-2660.
56. A. Galperin and S. Margel, *J Biomed Mater Res B*, 2007, **83B**, 490-498.
57. J. Ma, G. Sun, N. S. Lee, W. J. Du, K. L. Wooley, C. L. Kahakachchi, W. D. McGhee, J. McDonald, T. E. Rogers and D. A. Moore, *Abstr Pap Am Chem S*, 2010, **239**.
58. Z. Y. Wang, T. Chang, L. Hunter, A. M. Gregory, M. Tanudji, S. Jones and M. H. Stenzel, *Aust J Chem*, 2014, **67**, 78-84.
59. J. Chiefari, Y. K. Chong, F. Ercole, J. Krstina, J. Jeffery, T. P. T. Le, R. T. A. Mayadunne, G. F. Meijs, C. L. Moad, G. Moad, E. Rizzardo and S. H. Thang, *Macromolecules*, 1998, **31**, 5559-5562.
60. A. Gregory and M. H. Stenzel, *Prog Polym Sci*, 2012, **37**, 38-105.
61. C. Boyer, M. H. Stenzel and T. P. Davis, *J Polym Sci Pol Chem*, 2011, **49**, 551-595.
62. J. F. Lutz, *J Polym Sci Pol Chem*, 2008, **46**, 3459-3470.
63. D. J. Coles, B. E. Rolfe, N. R. B. Boase, R. N. Veedu and K. J. Thurecht, *Chemical Communications*, 2013, **49**, 3836-3838.
64. L. Tao, J. Q. Liu, B. H. Tan and T. P. Davis, *Macromolecules*, 2009, **42**, 4960-4962.
65. L. Zhang, W. G. Liu, L. Lin, D. Y. Chen and M. H. Stenzel, *Biomacromolecules*, 2008, **9**, 3321-3331.
66. F. H. Meng, W. E. Hennink and Z. Zhong, *Biomaterials*, 2009, **30**, 2180-2198.
67. C. Zhang, H. Peng and A. K. Whittaker, *Journal of Polymer Science Part A: Polymer Chemistry*, 2014, DOI: 10.1002/pola.27252, n/a-n/a.
68. K. Wang, H. Peng, K. J. Thurecht, S. Puttick and A. K. Whittaker, *Biomacromolecules*, 2015, **16**, 2827-2839.
69. N. Bloembergen, E. Purcell and R. Pound, *Phys Rev*, 1948, **73**, 679-712.
70. H. Yan, L. He, C. Ma, J. Li, J. Yang, R. Yang and W. Tan, *Chem Commun (Camb)*, 2014, **50**, 8398-8401.
71. J. H. Tan, N. A. J. McMillan, E. Payne, C. Alexander, F. Heath, A. K. Whittaker and K. J. Thurecht, *J Polym Sci Pol Chem*, 2012, **50**, 2585-2595.
72. T. Y. Zhao, Y. Zheng, J. Poly and W. X. Wang, *Nat Commun*, 2013, **4**.
73. G. Y. Wu, Y. Z. Fang, S. Yang, J. R. Lupton and N. D. Turner, *J Nutr*, 2004, **134**, 489-492.
74. M. Shilo, T. Reuveni, M. Motiei and R. Popovtzer, *Nanomedicine-Uk*, 2012, **7**, 257-269.
75. C. T. Badea, K. K. Athreya, G. Espinosa, D. Clark, A. P. Ghafoori, Y. F. Li, D. G. Kirsch, G. A. Johnson, A. Annapragada and K. B. Ghaghada, *Plos One*, 2012, **7**.
76. C. Y. Kao, E. A. Hoffman, K. C. Beck, R. V. Bellamkonda and A. V. Annapragada, *Acad Radiol*, 2003, **10**, 475-483.
77. X. Li, N. Anton, G. Zuber, M. J. Zhao, N. Messaddeq, F. Hallouard, H. Fessi and T. F. Vandamme, *Biomaterials*, 2013, **34**, 481-491.
78. F. Hallouard, S. Briancon, N. Anton, X. Li, T. Vandamme and H. Fessi, *Eur J Pharm Biopharm*, 2013, **83**, 54-62.
79. A. de Vries, E. Custers, J. Lub, S. van den Bosch, K. Nicolay and H. Grull, *Biomaterials*, 2010, **31**, 6537-6544.
80. K. E. Dekrafft, Z. G. Xie, G. H. Cao, S. Tran, L. Q. Ma, O. Z. Zhou and W. B. Lin, *Angew Chem Int Edit*, 2009, **48**, 9901-9904.

Multifunctional Hyperbranched Polymers for CT/^{19}F MRI Bimodal Molecular Imaging

Kewei Wang, Hui Peng, Kristofer J. Thurecht, Simon Puttick and Andrew K. Whittaker*

Australian Institute for Bioengineering and Nanotechnology; Centre for Advanced Imaging; ARC Centre of Excellence in Convergent Bio-Nano Science and Technology, The University of Queensland, St. Lucia, Queensland 4072, Australia
E-mail: a.whittaker@uq.edu.au; Fax: +61-7-33463973; Tel: +61-7-33463885

Multifunctional hyperbranched polymers containing iodine and fluorine were synthesised by reversible addition-fragmentation chain transfer (RAFT) polymerisation, and evaluated as novel contrast agents for CT/^{19}F MRI bimodal molecular imaging.